J Solid State Electrochem (2005) 9: 421–428
DOI 10.1007/s10008-004-0578-x

ORIGINAL PAPER

H. Chen · J. M. Wang · Y. L. Zhao · J. Q. Zhang
C. N. Cao

Electrochemical performance of Zn-substituted $Ni(OH)_2$ for alkaline rechargeable batteries

Received: 1 June 2004 / Accepted: 20 July 2004 / Published online: 1 December 2004

Abstract Zn-substituted $Ni(OH)_2$ for alkaline rechargeable batteries was prepared by a chemical coprecipitation method. The structures were characterized by X-ray diffraction and scanning electron microscopy, and the electrochemical performance, including charge–discharge behavior, the proton diffusion coefficient (D_{H+}), and the cycle life, was investigated in detail. The results showed that the charge–discharge potentials of Zn-substituted β-$Ni(OH)_2$ are much higher than those of Zn-substituted α-$Ni(OH)_2$. For a single α (for 30.5–48.4% Zn content) or a single β (from 0 to 9.3% Zn content) phase in the sample, the discharge potentials increase with the increase of Zn content. However, when there is an α and β phase mixture in the sample, the discharge potential decreases with an increase of Zn content. The D_{H+} values of Zn 0% and Zn 38.1% samples measured by the current-pulse relaxation method are much lower than those of Zn 9.3% and Zn 19.6% samples. D_{H+} of all the samples decreases with an increase of the depth of discharge. The effects of different Zn contents on the charge–discharge potentials of the nickel electrodes can be attributed to the differences of the electrochemical and diffusion polarization.

Keywords Zn-substituted α-$Ni(OH)_2$ · Electrochemical performance · Diffusion coefficient of proton

Introduction

Nickel hydroxide has been widely used as the positive electrode material of Ni–Cd, Ni–Fe, Ni–Zn, Ni–H_2 and Ni–MH rechargeable batteries. In commercial batteries, spherical β-$Ni(OH)_2$ powders are usually utilized since β-$Ni(OH)_2$ has a high tapping density (more than 2.0 g cm^{-3}) and good stability in strong alkaline electrolyte. However, there are two factors that inhibit its further improvement as the active material [1]:

1. The theoretical capacity of β-$Ni(OH)_2$ is 289 mA h g^{-1} owing to one-electron transportation in the β-$Ni(OH)_2$/β-NiOOH system, and this has been approximately reached in current commercial batteries.
2. γ-NiOOH is easily formed when β-$Ni(OH)_2$ is overcharged, which results in the swelling of the electrode volume by the intercalation of water molecules and metallic cations such as K^+ and causes rapid capacity fading during charge–discharge cycles.

Recently, more attention has been paid to α-$Ni(OH)_2$. For the α-$Ni(OH)_2$/γ-NiOOH couple, a larger discharge capacity can be obtained since the oxidation state of nickel in γ-NiOOH is 3.67 or 3.3–3.7 [2, 3] and there are no volume expansion and mechanical deformation problems. However, pure α-$Ni(OH)_2$ is unstable in a strong alkaline medium and easily transforms to β-$Ni(OH)_2$ [1]. Many efforts have been focused on the preparation of stabilized α-$Ni(OH)_2$ by partial substitution of Co [4], Al [5, 6, 7, 8, 9, 10], Fe [11], Mn [12] and Zn [13, 14] for Ni to increase the stability of the α-phase structure in a strong alkaline medium. When Ni^{2+} is substituted by other metal ions, excess positive charge is formed in the NiO_2 layers, which results in the intercalation of anions such as CO_3^{2-}, SO_4^{2-} and NO_3^- into the interlayer. So the electrostatic force between the layers inhibits the dissolution of NiO_2 layers and enhances the structural stabilization of α-$Ni(OH)_2$. The locations of various substitution metal ions in the $Ni(OH)_2$ lattice are different. Comprehensive studies [4, 11, 12] have shown that M^{3+} or Mn^{4+} occupies the Ni^{2+} position in $Ni(OH)_2$ lattice. The group of Tessier [13] found that for Zn-substituted α-$Ni(OH)_2$, zinc cations are located in tetrahedral sites of the interslab space; these tetrahedrals share one face with the octa-

H. Chen · J. M. Wang (✉) · Y. L. Zhao · J. Q. Zhang · C. N. Cao
Department of Chemistry, Zhejiang University,
310027 Hangzhou, People's Republic of China
E-mail: wjm@cmsce.zju.edu.cn
Tel.: +86-571-87951513
Fax: +86-571-87951358

J. Q. Zhang · C. N. Cao
Chinese State Key Laboratory for Corrosion and Protection,
110015 Shenyang, People's Republic of China

hedral vacancies within the slab. The existence of pairs of zinc cations located above and below the octahedral vacancies of the slab implies an excess of positive charge which is compensated by the intercalation of carbonate ions. It is predicted that the different structure of substituted α-$Ni(OH)_2$ will have different effects on the electrochemical performance. Previous work [13, 14] mostly focused on the study of the structural stabilization of Zn-substituted α-$Ni(OH)_2$ during ageing in alkaline solution. The electrochemical performance of Zn-substituted α-$Ni(OH)_2$ has not been investigated systematically.

In the present work, Zn-substituted $Ni(OH)_2$ was prepared by a chemical coprecipitation method. The effects of Zn content on the structure and electrochemical performance of $Ni(OH)_2$ samples were studied in detail.

Experimental

Preparation of samples

A NaOH solution containing Na_2CO_3 (2.5 g dm^{-3}) and a mixed solution of $NiSO_4$ and $ZnSO_4$, in a required $[Zn^{2+}]/([Zn^{2+}]+[Ni^{2+}])$ ratio, were slowly added to a well-sealed reaction vessel with 250 cm^3 aqueous ammonia solution (1.0 mol dm^{-3}) at the same feeding speed under vigorous stirring. The reaction temperature was maintained at 55 ± 1 °C, and the pH of the reaction solution was held at 11.0 ± 0.1. After the precipitation reaction had been undertaken for 6–8h, the reaction product was aged in the mother solution for another 16 h at 55 °C. The product was filtered off, washed several times with deionized water until the solution was to neutral, and dried at 60 °C in air.

Characterization of nickel hydroxide

The chemical compositions (Ni and Zn contents) were measured by an inductively coupled argon plasma emission spectrophotometer (ICP, IRIS Intrepid II XSP, Thermo Electron Corporation, USA). The structures of the samples were determined using an X-ray diffractometer (Rigaku D/Max 2550), with Cu Kα radiation at 40 kV, 300 mA. The morphology of the samples was examined using scanning electron microscopy (SEM) (Philips XL 30 ESEM).

Preparation of electrodes and electrochemical tests

The pasted nickel electrodes were prepared as follows. The sample (90 wt%), cobalt powder (5 wt%) and graphite powder (5 wt%) were thoroughly mixed with a certain amount of 5% poly(tetrafluoroethylene) solution. The paste obtained was incorporated into nickel foam (2 cm×2 cm×0.9 mm) with a spatula. The pasted nickel electrodes were dried at 50 °C and then roll-pressed to a thickness of 0.5 mm. Thereafter, the electrodes were soaked in 6 mol dm^{-3} KOH for 24 h before being coupled with porous Ni electrodes on either side as counters and a Hg/HgO electrode as a reference. Galvanostatic charge–discharge studies were conducted using a DC-5 cell performance-testing instrument (made in China). The working electrode was galvanostatically charged at 0.1 C for 15 h, rested for 5 min, and then discharged to 0.1 V versus Hg/HgO at 0.1 C for five activation cycles. Cycle performance was tested under the following scheme: charge at 1.0 C for 1.4 h, rest for 5 min, and discharge at 1.0 C to 0.1 V versus Hg/HgO. Electrochemical impedance spectroscopy (EIS) measurements were performed using a model 273A potentiostat/galvanostat in conjunction with a model 5210 lock-in amplifier.

The proton diffusion coefficient (D_{H+}) in nickel electrodes was measured by the current-pulse relaxation (CPR) technique described by Kumagai et al. [15] and Watanabe and coworkers [16, 17] using the following formula for the time dependence of the transient potential (ΔE):

$$\Delta E = IV_m\tau(dE/dn)\Big/FA(\pi D_{H^+}t)^{1/2}, \quad (1)$$

where I is a current pulse (300 mA), V_m is the molar volume (31.83 and 22.61 cm^3 for α-$Ni(OH)_2$ and β-$Ni(OH)_2$, respectively [16, 17]), τ is the duration of the pulse (8 s), (dE/dn) is the slope of the open-circuit potential (OCP) as a function of capacity, and A is the apparent geometric area (4 cm^2), which is assumed to be true in the present work. The equilibrium OCP was measured after about 24 h on open circuit. In Eq. (1), $n = 0$–2 is used by assuming the following electrode reaction:

$$NiOOH_x \leftrightarrow NiOOH_{x-n} + nH^+ + ne^- (x = 0-2,\ n = 0-2). \quad (2)$$

These CPR tests were conducted on the Arbin BT-2000 system. All the electrochemical tests were carried out at room temperature. The specific discharge capacity in this paper is in terms of the capacity per gram of pure $Ni(OH)_2$.

Results and discussion

Structure and morphology of the samples

The Zn-substituted nickel hydroxide samples are named as Zn C%, where C is the mole percentage of Zn versus the total number of moles of Ni and Zn in the samples measured by ICP tests. Powder X-ray diffraction (XRD) patterns of the Zn-substituted $Ni(OH)_2$ samples are shown in Fig. 1. It can be seen that the samples show different phase structures with an increase of Zn content.

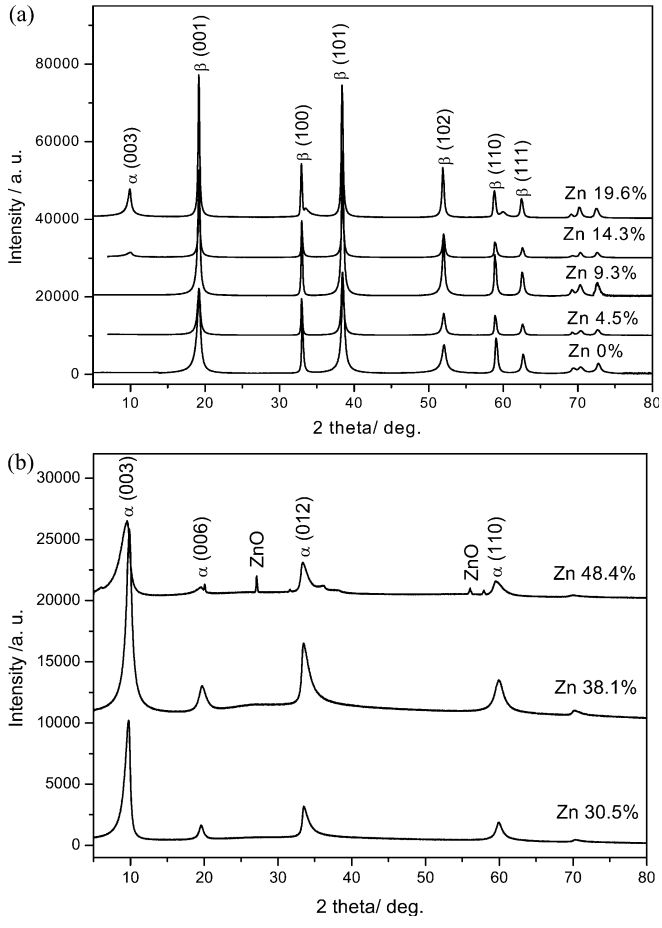

Fig. 1 X-ray diffraction patterns of Zn-substituted $Ni(OH)_2$ samples

The samples manifest the features of the β-$Ni(OH)_2$ phase (JCPDS 14–117) when the Zn content is less than 14.3%. When the content is 14.3%, a peak at $2\theta = 10.04°$ appears, which is characteristic of the α-$Ni(OH)_2$ phase (JCPDS 38–715), and there is a mixture of α and β phases. When the Zn content increases continuously, the samples show a single α phase (Zn 30.5% and Zn 38.1%). The prerequisite Zn content to form a single α-$Ni(OH)_2$ phase is much higher than the content of other metal ions in substituted α-$Ni(OH)_2$ samples such as Al [5, 6, 7, 8, 9, 10], Fe [11] and Mn [12], which is properly due to the different locations of substituted ions in the $Ni(OH)_2$ lattice. For Al-substituted α-$Ni(OH)_2$, Al^{3+} occupies the Ni position in the $Ni(OH)_2$ lattice and one excess positive charge is formed when one Ni position is occupied by Al^{3+}. However, for Zn-substituted α-$Ni(OH)_2$, a pair of zinc cations locate above and below the octahedral vacancies of the NiO_2 slabs, and form one excess positive charge. For the Zn 48.4% sample, diffraction lines for the ZnO phase appear together with lines of the α-$Ni(OH)_2$ phase. This amount of zinc is thus beyond the solid solution domain of the α-type phase. To obtain a single Zn-substituted α-$Ni(OH)_2$ sample, the zinc content should be chosen in an appropriate range.

The d values and the full widths at half maximum (FWHM) of (001) and (003) planes for β and α phases, respectively, of the samples are listed in Table 1. For the Zn-substituted β-$Ni(OH)_2$ sample, the $d_{(001)}$ value remains almost unchanged and the $FWHM_{(001)}$ decreases dramatically with the increase of Zn content, which indicates that the coprecipitation of Zn improves the crystallinity and has no effect on the interlayer distance of β-$Ni(OH)_2$. For Zn-substituted α-$Ni(OH)_2$, the $d_{(003)}$ and $FWHM_{(003)}$ values both increase with the increase of Zn content. In the substituted α-$Ni(OH)_2$ sample, large numbers of anions such as SO_4^{2-} and CO_3^{2-} are intercalated into the interlayer. The higher the Zn content in α-$Ni(OH)_2$ is, the more anions are intercalated, and the interlayer distance becomes larger. The turbostratic structure in the interlayer becomes more disordered and the crystallinity decreases, which leads to the increase of $FWHM_{(003)}$ with the increase of Zn content.

Figure 2 shows the SEM photographs of several typical samples at different magnifications. At low magnification, the Zn 0% sample shows spherical particles and the aggregates of some quasispherical particles. The average diameter of the particles is about 10 μm. On magnification, the surface structure can be seen clearly. The surface is not smooth and the tapping of crystallite forms the sheet. The crystallite can be seen from the edge of the sheets. The degree of sphericity and uniformity of the particle size of the Zn 9.3% sample are obviously very low and the shape of the particle is very irregular. At high magnification, crossed agglomerations of crystallites and a porous cagelike structure appear, which makes the penetration of electrolyte and the diffusion of protons in the sample much easier and increases the electrochemical activity of the nickel electrode. The Zn 38.1% sample manifests a more irregular shape and a smaller particle size. Moreover, the surface of the sample is much looser than the surfaces of the Zn 0% and Zn 9.3% samples. It can be concluded that the degree of sphericity and the average size are decreased and the growth and tapping of crystallites become disordered with the increase of Zn content in the $Ni(OH)_2$ samples.

Table 1 The d values and full width at half maximum ($FWHM$) in (001) and (003) planes of the samples

	Zn 0%	Zn 4.5%	Zn 9.3%	Zn 14.3%	Zn 19.6%	Zn 30.5%	Zn 38.1%	Zn 48.4%
$d_{(001)}$	4.616	4.624	4.614	4.614	4.619			
$d_{(003)}$				8.803	8.928	9.055	9.000	9.244
$FWHM_{(001)}$	0.669	0.446	0.329	0.262	0.233			
$FWHM_{(003)}$				0.999	0.642	0.867	1.044	1.520

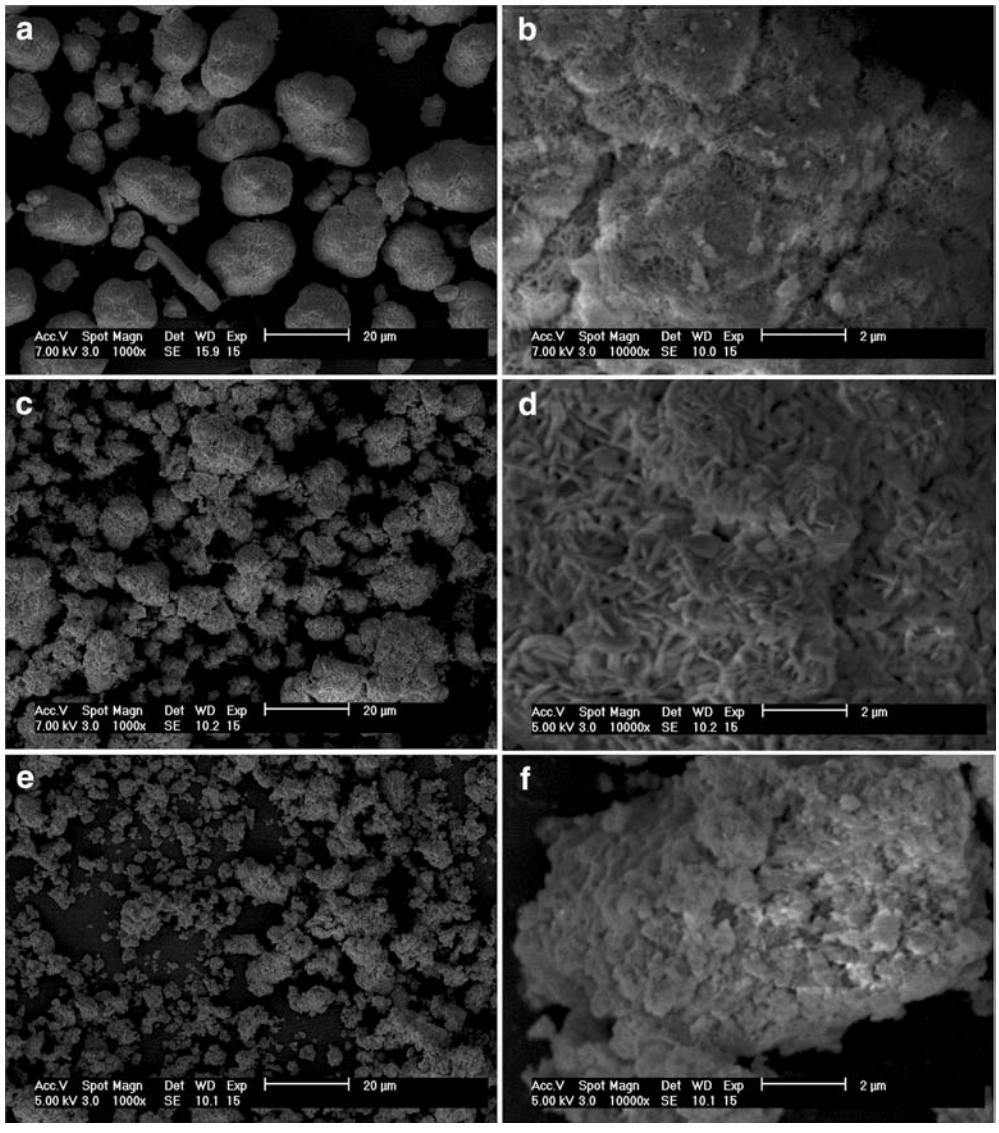

Fig. 2 Scanning electron microscope photos of different samples: **a**, **b** Zn 0%; **c**, **d** Zn 9.3%; **e**, *f* Zn 38.1%

Electrochemical performance of the samples

Galvanostatic charge-discharge

Figure 3 shows the charge–discharge curves of nickel hydroxide electrodes with different Zn contents at 1.0 C for the first cycle. Zn-substituted β-$Ni(OH)_2$ and Zn-substituted α-$Ni(OH)_2$ electrodes show different charge–discharge curves. The charge and discharge potentials of Zn-substituted β-$Ni(OH)_2$ electrodes increase with the increase of Zn content and they are higher than those of Zn-substituted α-$Ni(OH)_2$ electrodes. Figure 4 shows the effects of Zn content on the half-discharge potential (E_{hd}, defined as the potential at the half-discharge capacity), the oxygen evolution potential (E_{ox}), the difference between E_{ox} and E_{hc} (defined as the potential at the half-charge capacity before reaching the potential plateau of oxygen evolution), and the potential difference (E_{diff}) between the half-charge potential E_{hc} and E_{hd} at 0.1 and 1.0 C. It could be seen that E_{hd} increases

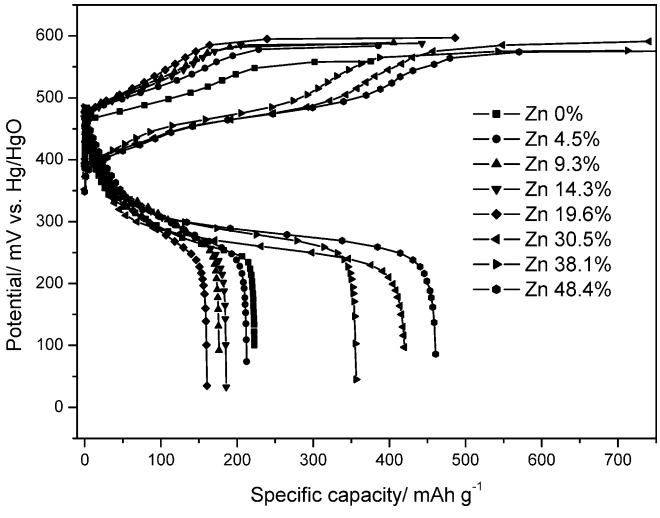

Fig. 3 Charge–discharge curves of Zn-substituted $Ni(OH)_2$ samples at 1.0 C

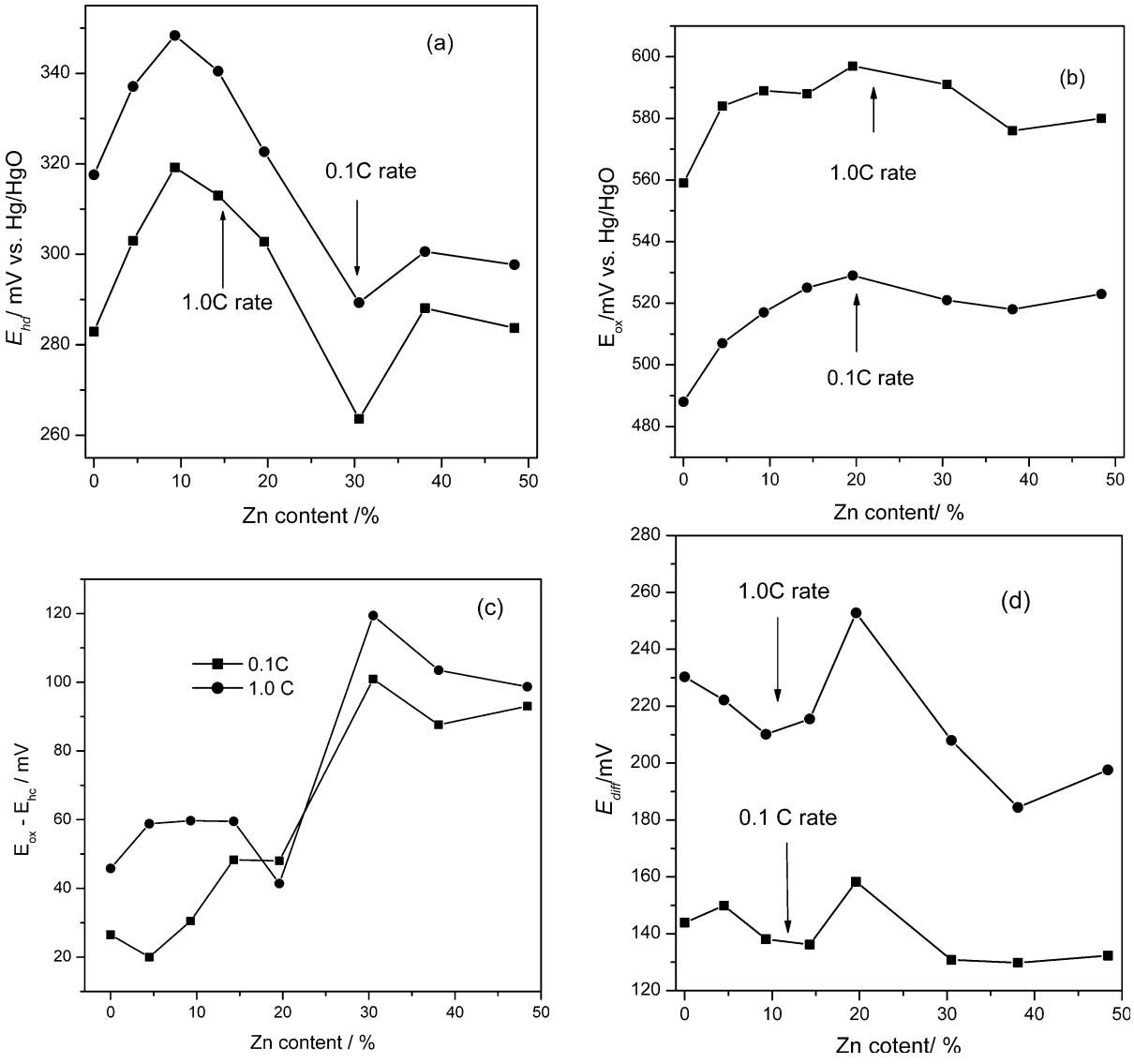

Fig. 4 **a** E_{hd}, **b** E_{ox}, **c** $E_{ox}-E_{hc}$ and **d** E_{diff} of Zn-substituted $Ni(OH)_2$ at 0.1 and 1.0 C

with the increase of Zn content when the Zn content is less than 9.3%. When the α phase appears in the sample (such as in the Zn 14.3% sample), E_{hd} decreases with the increase of Zn content. E_{hd} reaches the lowest value at Zn 30.5%, which is the single α-$Ni(OH)_2$ phase. When the Zn content is more than 30.5%, E_{hd} of the sample increases slightly.

The effects of Zn content on the E_{hd} value of nickel electrodes are completely different from those of other metal-substituted $Ni(OH)_2$ samples such as Mn, Co, Fe and Al [5, 6, 7, 8, 9, 10, 11, 12]. Based on the difference in size between the substitution cation and the nickel ion in the γ phase, a model has been proposed by Guerlou-Demourgues et al. [12] to interpret the effect of the substitution cation on the potential of the nickel electrode. It conforms quite well with the experimental results of Mn-, Co- and Fe-substituted nickel hydroxide. The smaller size of the Mn^{4+} ion, $r(Mn^{4+})=0.54$ Å [18], against that of the Ni^{3+} one, $r(Ni^{3+})=0.56$ Å [18], induces a decrease in the electrode potential with increasing substitution amount, similarly for the cobalt system, whereas in the case of the Fe-substituted material the larger size of the Fe^{3+} and Fe^{4+} ions, $r(Fe^{3+})=0.64$ Å and $r(Fe^{4+})=0.59$ Å [18], entails an increase in the potential. But the potential of Al-substituted $Ni(OH)_2$ is not decreased owing to the smaller radius of Al^{3+}, $r(Al^{3+})=0.54$ Å [18], than that of Ni^{3+} [10]. This model cannot interpret the effect of Zn substitution on the potential of electrodes either. We consider that the potential is influenced not only by the radii of the substitution ions but also by the ratio of the α and β phases in the sample. The pure α/γ system has a lower reversible potential compared with the pure β/β system [3]. Although the radius of Zn^{2+}, $r(Zn^{2+})=0.74$ Å [18], is larger than that of Ni^{3+}, the discharge potential decreases with the increase of Zn content in the range from 9.3 to 30.5% owing to the increase of the α phase content. The different effects between Zn-substituted $Ni(OH)_2$ and other

M-substituted $Ni(OH)_2$ (*M* is Fe, Mn and Co) on the potentials of nickel electrodes are probably due to the different locations of substitution ions in the $Ni(OH)_2$ lattice. Fe, Mn and Co ions only occupy the Ni positions; however, Zn^{2+} not only occupies the Ni position, but also exists as a pair of zinc cations above and below the octahedral vacancies of the slabs when there is the mixture of α and β phases in the sample [13]. For the samples with a single α (30.5–48.4% Zn substitution amounts) or β phase (0–9.3% Zn substitution amounts), the discharge potentials both increase with the increase of Zn content, which is in coincidence with the previously-mentioned model.

The E_{ox} value of the Zn-substituted $Ni(OH)_2$ sample first increases and then decreases with the increase of Zn content. E_{ox} reaches the maximum value at 19.6% Zn. The $E_{ox}-E_{hc}$ value can influence the charge efficiency and the discharge capacity of the nickel electrode. It can be seen from Fig. 4c that the E_{ox}–E_{hc} values of Zn-substituted α-$Ni(OH)_2$ samples are much higher than those of Zn-substituted β-$Ni(OH)_2$, which means that the former have a higher discharge capacity than the latter. E_{diff} is a characteristic of the electrode polarization. E_{diff} of the nickel electrodes decreases at first and then increases. It also reaches the maximum value at 19.6% Zn. When the zinc content in the samples is larger than 19.6%, E_{diff} starts to decrease with the increase of Zn content. These results are the conjunct result of electrochemical polarization and diffusion polarization in the electrode reactions.

The cycle performance of $Ni(OH)_2$ samples with different Zn contents at 1.0C is shown in Fig. 5. It is obvious that the specific discharge capacity of Zn-substituted α-$Ni(OH)_2$ is much higher than that of Zn-substituted β-$Ni(OH)_2$, which accords with the earlier result of the $E_{ox}-E_{hc}$ values. The specific discharge capacity of Zn-substituted β-$Ni(OH)_2$ decreases with the increase of Zn content. When the sample contains an α phase, the specific discharge capacity increases with the increase of Zn content owing to the large discharge capacity of α-$Ni(OH)_2$. The discharge capacity of the Zn 48.4% sample is the highest and it exceeds 500 mA h g^{-1}. The discharge capacity of all the samples increases in the initial 100 cycles, and a greater increase in the discharge capacity is observed for the Zn 14.3% and Zn 19.6% samples. These two samples contain a mixture of α-$Ni(OH)_2$ and β-$Ni(OH)_2$, while the other Zn-containing samples are constituted from pure α-$Ni(OH)_2$ or pure β-$Ni(OH)_2$. The greater initial increase in discharge capacity observed for the samples with 14.3 and 19.6% of Zn is probably due to the presence of the mixture of both $Ni(OH)_2$ phases in the samples. After 100 cycles, the decrease in the discharge capacity of the samples with higher Zn content (larger than 38.1%) might result from the removal of Zn from the $Ni(OH)_2$ structure and the partial transformation of α-$Ni(OH)_2$ to β-$Ni(OH)_2$.

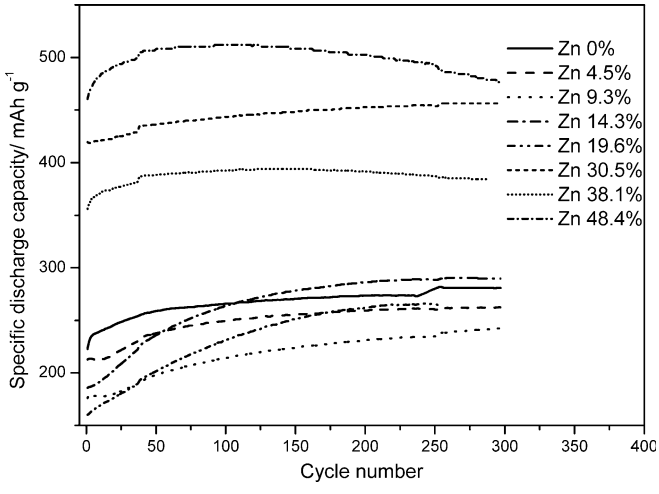

Fig. 5 The cycle performance of $Ni(OH)_2$ samples with different Zn contents at 1.0 C

Tests of the proton diffusion coefficient

In order to verify the diffusion polarization of the electrode, the proton diffusion coefficient (D_{H+}) was measured by the current pulse relaxation method. The closed-circuit potential and quasiequilibrium open-circuit potential are presented in Fig. 6a as a function of discharge capacity for the Zn 38.1% sample. When the current is interrupted after discharging to various capacities, the potentials of the nickel electrode recover gradually towards the equilibrium state. This is caused by a slow diffusion of protons from the electrode surface towards the bulk [15, 16, 17]. A typical transient voltage (ΔE) of the Zn 38.1% sample observed after the passage of a current pulse at 60% depth of discharge (DOD, the ratio of the actual discharge capacity at different conditions to the actual discharge capacity discharging to 0.1 V versus Hg/HgO) is plotted against $t^{-1/2}$ in Fig. 6b. The slope of the linear region can be used to calculate D_{H+} in the nickel hydroxide electrodes using Eq. (1).

Table 2 lists the D_{H+} values of the Zn 0%, Zn 9.3%, Zn 19.6% and Zn 38.1% samples at different DOD. The D_{H+} values of Zn 0% and Zn 38.1% are 1–3 magnitudes lower than those of the Zn 9.3% and Zn 19.6% samples. D_{H+} of Zn 9.3% reaches the maximum value at 20% DOD. D_{H+} values of all samples decrease with the increase of the DOD, which is completely different behavior from that of the Al-substituted α-$Ni(OH)_2$ electrode [19]. The difference probably results from the different location of the substitution metal in the $Ni(OH)_2$ lattice and the different properties of Zn^{2+} and Al^{3+}.

Electrochemical impedance spectroscopy

In order to study the effects of Zn on the kinetics process of the electrode, the electrochemical impedance spectra of the electrodes using Zn 0%, Zn 9.3%, Zn 19.6% and Zn 38.1% samples were measured at different DOD and the EIS patterns of all sample at 0% DOD are

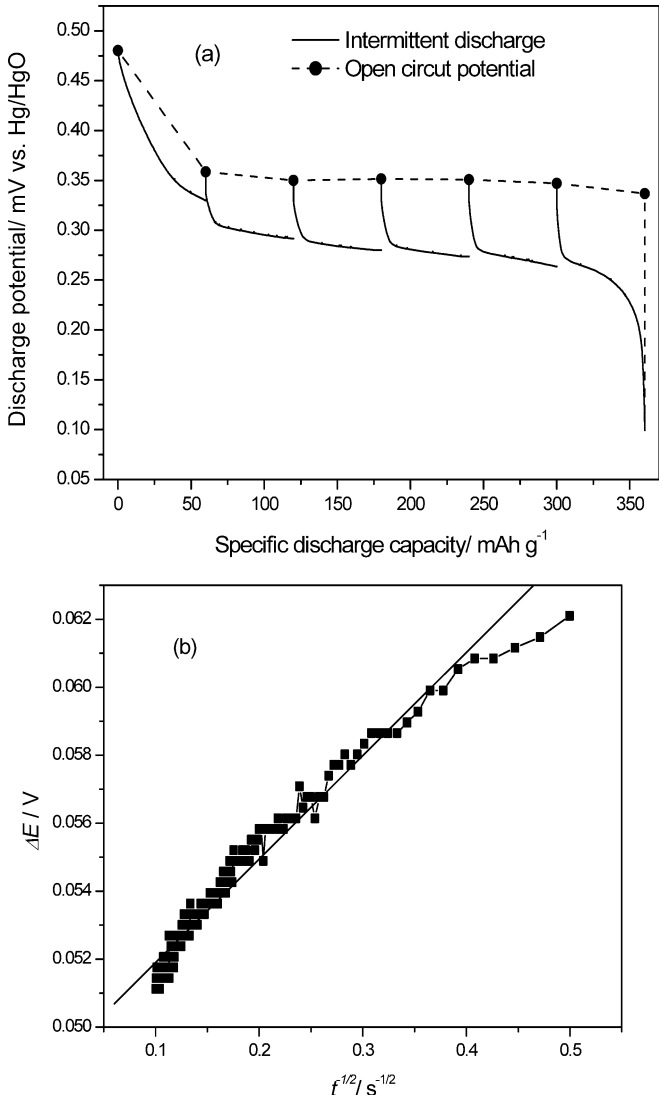

Fig. 6 a Closed-circuit and open-circuit potentials as a function of discharge capacity of the Zn 38.1% sample. **b** Typical plot of observed voltage (ΔE) against $t^{-1/2}$ for the Zn 38.1% sample at 60% depth of discharge (DOD)

Table 2 Depth of discharge (DOD) dependence of the proton diffusion coefficient ($cm^2\ s^{-1}$) for different samples

DOD (%)	Zn 0%	Zn 9.3%	Zn 19.6%	Zn 38.1%
0	5.74E−11	1.29E−08	1.16E−08	3.57E−10
20	3.64E−11	1.64E−08	1.42E−08	2.90E−10
40	3.38E−11	1.38E−08	1.34E−08	2.58E−10
60	4.53E−11	8.32E−09	8.50E−09	2.60E−10
80	4.36E−11	4.96E−09	5.53E−09	2.32E−10
100	2.80E−11	1.14E−09	2.35E−09	1.01E−10

displayed in Fig. 7a. The model for the essential features of the electrode is represented by the electrical equivalent circuit shown in Fig. 7b, where R_s is the total ohmic resistance of the solution, CPE is the constant phase element related to the double layer capacity, R_t is the charge-transfer resistance of the electrodes and W_o is the

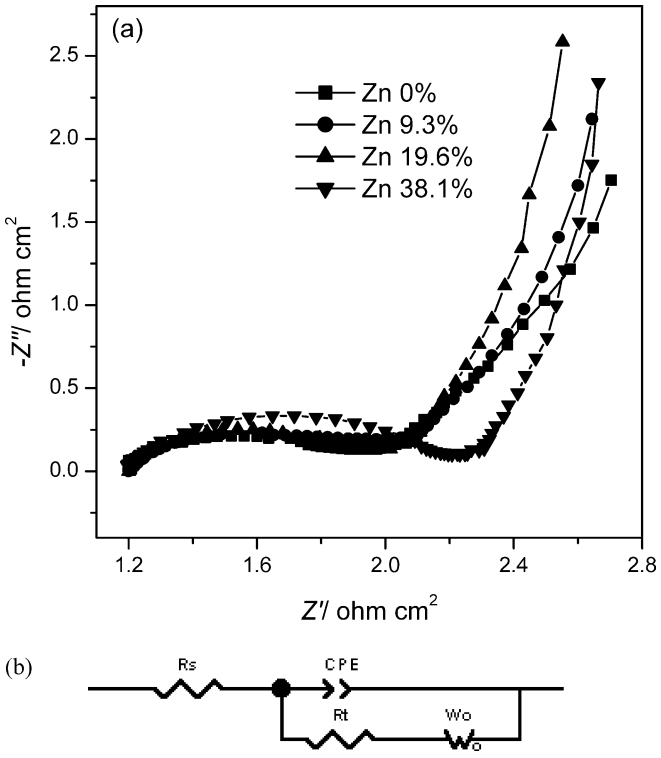

Fig. 7 a Typical Nyquist plots of different samples at 0% DOD. **b** Equivalent circuit for nickel electrodes

generalized finite Warburg impedance (Z_w) of the solid-phase diffusion. From the fitting results of R_t (shown in Table 3), it can be seen that R_t decreases at first and then increases with the increase of the Zn content at the same DOD except for 0% DOD. The results of the proton diffusion coefficient show that D_{H+} increases at first and then decreases with the increase of Zn content. As a result of electrochemical polarization and diffusion polarization, the half-discharge potential and E_{diff} increase at first and then decrease with the increase of Zn content, which is accordant with the results of galvanostatic charge–discharge experiments. For each sample, R_t increases with the increase of the DOD owing to the reduction of NiOOH and the increase of electrochemical polarization in the nickel electrode.

Conclusions

1. The Zn-substituted $Ni(OH)_2$ samples for alkaline rechargeable batteries were prepared by a chemical coprecipitation method. The single α-$Ni(OH)_2$ sample can be obtained when the Zn content is over 30.5%. When the Zn content is 48.4%, the ZnO phase appears in the sample owing to the oversaturation of solid dissolution of Zn in the lattice. For the Zn-substituted β-$Ni(OH)_2$ sample, the $d_{(001)}$ value almost remains unchanged and the $FWHM_{(001)}$ decreases dramatically with the increase of Zn content. However, for Zn-substituted α-$Ni(OH)_2$, $d_{(003)}$ and

Table 3 DOD dependence of R_t (Ω cm^2) for different samples

DOD (%)	Zn 0%	Zn 9.3%	Zn 19.6%	Zn 38.1%
0	0.65636	0.69304	0.68272	0.96732
25	0.79780	0.72500	0.55052	0.85988
50	1.48796	0.72860	0.68956	1.28480
75		1.20068	0.80612	

$FWHM_{(003)}$ both increase with the increase of Zn content. The degree of sphericity and crystallinity of $Ni(OH)_2$ samples both decrease with the increase of Zn content.

2. The charge and discharge potentials of Zn-substituted β-$Ni(OH)_2$ are much higher than those of Zn-substituted α-$Ni(OH)_2$. For the samples with a single α (30.5–48.4% Zn substitution amount) or a single β phase (0–9.3% Zn substitution amounts), the discharge potentials increase with the increase of Zn content. The specific discharge capacity of Zn-substituted α-$Ni(OH)_2$ is much higher than that of Zn-substituted β-$Ni(OH)_2$.
3. The D_{H+} values of Zn 0% and Zn 38.1% are much lower than those of Zn 9.3% and Zn 19.6% samples. The D_{H+} values of all the samples decrease with increase of the DOD. The charge transfer resistance of the samples decreases at first and then increases with the increase of Zn content at the same DOD. The electrochemical polarization and diffusion polarization result in the effects of Zn content on the charge–discharge potentials of the nickel electrodes.

Acknowledgements This work was supported by National Natural Science Foundation of China (approval no. 59902004). The authors also gratefully acknowledge the financial support of the Chinese State Key Laboratory for Corrosion and Protection.

References

1. Bode H, Dehmelt K, Witte J (1966) Electrochim Acta 11:1079
2. Corringan D, Knight SL (1989) J Electrochem Soc 136:613
3. Barnard R, Randell CF, Tye FF (1980) J Appl Electrochem 10:109
4. Faure C, Delmas C, Willmann P (1991) J Power Sources 36:497
5. Kamath PV, Dixit M, Indira L (1994) J Electrochem Soc 141:2956
6. Sugimoto A, Ishida S, Hanawa K (1999) J Electrochem Soc 146:1251
7. Liu B, Wang XY, Yuan HT, Zhang YS, Song DY, Zhou ZX (1999) J Appl Electrochem 29:855
8. Leng YJ, Liu B, Wang FJ, Zhou JX, Xiao Y, Ma ZF (2000) Chin J Power Sources 24:326
9. Wang CY, Zhong S, Konstantinov K, Walter G, Liu HK (2002) Solid State Ionics 148:503
10. Hu WK, Noreus D (2003) Chem Mater 15:974
11. Guerlou-Demourgues L, Delmas C (1993) J Power Sources 45:281
12. Guerlou-Demourgues L, Delmas C (1996) J Electrochem Soc 143: 561
13. Tessier C, Guerlou-Demourgues L, Faure C, Basterreix M, Nabias G, Delmas C (2000) J Mater Chem 10:1185
14. Tessier C, Guerlou-Demourgues L, Faure C, Basterreix M, Nabias G, Delmas C (2000) Solid State Ionics 133:11
15. Kumagai N, Tanifuji S, Fujiwara T, Tanno K (1992) Electrochim Acta 37:1039
16. Watanabe K, Kikuoka T (1995) J Appl Electrochem 25:219
17. Watanabe K, Koseki M, Kumagai N (1996) J Power Sources 58:23
18. Dean JA (1999) Lange's handbook of chemistry, 15th edn. McGraw-Hill, New York, p 4.29
19. Chen H, Wang JM, Pan T, Zhao YL, Zhang JQ, Cao CN (2003) J Electrochem Soc 11:A1399